

Variational Multiscale Proper Orthogonal Decomposition: Navier-Stokes Equations

Traian Iliescu¹ and Zhu Wang^{*2}

¹Department of Mathematics, Virginia Polytechnic Institute and State University,
Blacksburg, VA 24061-0123, U.S.A.

²Institute for Mathematics and its Applications, University of Minnesota, Minneapolis,
MN 55455-0134, U.S.A.

Revision 1 – September 4, 2018

Abstract

We develop a variational multiscale proper orthogonal decomposition reduced-order model for turbulent incompressible Navier-Stokes equations. The error analysis of the full discretization of the model is presented. All error contributions are considered: the spatial discretization error (due to the finite element discretization), the temporal discretization error (due to the backward Euler method), and the proper orthogonal decomposition truncation error. Numerical tests for a three-dimensional turbulent flow past a cylinder at Reynolds number $Re = 1000$ show the improved physical accuracy of the new model over the standard Galerkin and mixing-length proper orthogonal decomposition reduced-order models. The high computational efficiency of the new model is also showcased. Finally, the theoretical error estimates are confirmed by numerical simulations of a two-dimensional Navier-Stokes problem.

Keywords. Proper orthogonal decomposition, variational multiscale, reduced-order model, finite element method.

*Corresponding author (wangzhu@ima.umn.edu).

1 Introduction

Due to the complexity of fluid flows in many realistic engineering problems, millions or even billions of degrees of freedom are often required in a direct numerical simulation (DNS). To allow efficient numerical simulations in these applications, reduced-order models (ROMs) are often used. The proper orthogonal decomposition (POD) has been one of the most popular approaches employed in developing ROMs for complex fluid flows [2, 25, 30, 31, 32]. It starts by using a DNS (or experimental data) to generate a POD basis $\{\varphi_1, \dots, \varphi_d\}$ that maximizes the energy content in the system, where d is the rank of the data set. By utilizing the Galerkin method, one can project the original system onto the space spanned by only a handful of dominant POD basis functions $\{\varphi_1, \dots, \varphi_r\}$, with $r \leq d$, which results in a low-order model — the Galerkin projection-based POD-ROM (POD-G-ROM).

The POD-G-ROM has been applied successfully in the numerical simulation of laminar flows. It is well known, however, that a simple POD-G-ROM will generally produce erroneous results for turbulent flows [3]. The reason is that, although the discarded POD modes $\{\varphi_{r+1}, \dots, \varphi_d\}$ only contain a small part of the system's kinetic energy, they do, however, have a significant impact on the dynamics. To model the effect of the discarded POD modes, various approaches have been proposed (see, e.g., the survey in [37]). In this report, we develop an approach that improves the physical accuracy of the POD-ROM for turbulent incompressible fluid flows by utilizing a variational multiscale (VMS) idea [14, 15]. This method is an extension to the Navier-Stokes equations (NSE) of the VMS-POD-ROM that we proposed in [16] for convection-dominated convection-diffusion-reaction equations. Our approach employs an eddy viscosity (EV) to model the interaction between the discarded POD modes and those retained in the POD-ROM. Instead of being added to all the resolved POD modes $\{\varphi_1, \dots, \varphi_r\}$, EV is only added to the small resolved scales (POD modes $\{\varphi_{R+1}, \dots, \varphi_r\}$ with $R < r$) in the VMS-POD-ROM. Thus, the small scale oscillations are eliminated without polluting the large scale components of the approximation. The small scales in the VMS-POD-ROM are defined by a projection approach in [16], which is also used in [17, 18, 19, 20, 23] in the finite element (FE) context. We also note that a different approach was developed in [9, 10].

In this report, the VMS-POD-ROM is extended and studied for the NSE. A rigorous error

51 analysis of the full discretization of the model (FE in space, backward Euler in time) is presented.
 52 A numerical test of the VMS-POD-ROM for three-dimensional (3D) turbulent flow past a circular
 53 cylinder at Reynolds number $\text{Re} = 1000$ is conducted to investigate the physical accuracy of
 54 the model. The theoretical error estimates are confirmed by using the VMS-POD-ROM in the
 55 numerical simulation of a two-dimensional (2D) flow.

56 The rest of this paper is organized as follows: In Section 2, we briefly describe the POD
 57 methodology and introduce the new VMS-POD-ROM. The error analysis for the full discretization
 58 of the new model is presented in Section 3. The new methodology is tested numerically in Section
 59 4 for a 3D flow past a circular cylinder and a 2D flow problem. Finally, Section 5 presents the
 60 conclusions and future research directions.

61 2 Variational Multiscale Proper Orthogonal Decomposition

62 We consider the numerical solution of the incompressible Navier-Stokes equations:

$$\left\{ \begin{array}{ll} \mathbf{u}_t - \nu \Delta \mathbf{u} + (\mathbf{u} \cdot \nabla) \mathbf{u} + \nabla p = \mathbf{f}, & \text{in } \Omega \times (0, T], \\ \nabla \cdot \mathbf{u} = 0, & \text{in } \Omega \times (0, T], \\ \mathbf{u} = 0, & \text{on } \partial\Omega \times (0, T], \\ \mathbf{u}(\mathbf{x}, 0) = \mathbf{u}^0(\mathbf{x}), & \text{in } \Omega, \end{array} \right. \quad (2.1)$$

63 where $\mathbf{u}(\mathbf{x}, t)$ and $p(\mathbf{x}, t)$ represent the fluid velocity and pressure of a flow in the region Ω , respec-
 64 tively, for $\mathbf{x} \in \Omega$, $t \in [0, T]$, and $\Omega \subset \mathbb{R}^n$ with $n = 2$ or 3 ; the flow is bounded by walls and driven by
 65 the force $\mathbf{f}(\mathbf{x}, t)$; ν is the reciprocal of the Reynolds number; and $\mathbf{u}^0(\mathbf{x})$ denotes the initial velocity.
 66 We also assume that the boundary of the domain, $\partial\Omega$, is polygonal when $n = 2$ and is polyhedral
 67 when $n = 3$.

The following functional spaces and notations will be used in the paper:

$$\mathbf{X} = \mathbf{H}_0^1(\Omega) = \{ \mathbf{v} \in [L^2(\Omega)]^n : \nabla \mathbf{v} \in [L^2(\Omega)]^{n \times n} \text{ and } \mathbf{v} = \mathbf{0} \text{ on } \partial\Omega \},$$

$$Q = L_0^2(\Omega) = \left\{ q \in L^2(\Omega) : \int_{\Omega} q \, d\mathbf{x} = 0 \right\},$$

$$\mathbf{V} = \{ \mathbf{v} \in \mathbf{X} : (\nabla \cdot \mathbf{v}, q) = 0, \forall q \in Q \}, \text{ and}$$

$$\mathbf{V}^h = \left\{ \mathbf{v}_h \in \mathbf{X}^h : (\nabla \cdot \mathbf{v}_h, q_h) = 0, \forall q_h \in Q^h \right\},$$

68 where $\mathbf{X}^h \subset \mathbf{X}$ and $Q^h \subset Q$ are the FE spaces of the velocity and pressure, respectively. In
 69 what follows, we consider the div-stable pair of FE spaces $\mathbb{P}^m/\mathbb{P}^{m-1}$, $m \geq 2$ [24]. That is, the
 70 FE approximation of the velocity is continuous on Ω and is an n -vector valued function with each
 71 component a polynomial of degree less than or equal to m when restricted to an element, while
 72 that of the pressure is also continuous on Ω and is a single valued function that is a polynomial of
 73 degree less than or equal to $m - 1$ when restricted to an element. We emphasize, however, that our
 74 analysis extends to more general FE spaces. We consider the following spaces for the POD setting:

$$\mathbf{X}^r := \text{span} \{ \varphi_1, \varphi_2, \dots, \varphi_r \}, \quad (2.2a)$$

$$\mathbf{X}^R := \text{span} \{ \varphi_1, \varphi_2, \dots, \varphi_R \}, \text{ and} \quad (2.2b)$$

$$\mathbf{L}^R := \text{span} \{ \nabla \varphi_1, \nabla \varphi_2, \dots, \nabla \varphi_R \}, \quad (2.2c)$$

75 where φ_j , $j = 1, \dots, r$, are the POD basis functions that will be defined in Section 2.1. We note
 76 that $\mathbf{X}^R \subset \mathbf{X}^r$, since $R < r$.

77 We introduce the following notations: Let \mathcal{H} be a real Hilbert space endowed with inner product
 78 $(\cdot, \cdot)_{\mathcal{H}}$ and norm $\| \cdot \|_{\mathcal{H}}$. Let the trilinear form $b^*(\cdot, \cdot, \cdot)$ be defined as

$$b^*(\mathbf{u}, \mathbf{v}, \mathbf{w}) = \frac{1}{2} [((\mathbf{u} \cdot \nabla) \mathbf{v}, \mathbf{w}) - ((\mathbf{u} \cdot \nabla) \mathbf{w}, \mathbf{v})]$$

79 and the norm $\| \cdot \|$ be defined as $\| \mathbf{v} \|_{s,k} := \left(\frac{1}{M} \sum_{i=0}^{M-1} \| \mathbf{v}(\cdot, t_{i+1}) \|_k^s \right)^{1/s}$, where s and M are positive
 80 integers.

81 The weak formulation of the NSE (2.1) reads: Find $\mathbf{u} \in \mathbf{X}$ and $p \in Q$ such that

$$\begin{cases} (\mathbf{u}_t, \mathbf{v}) + \nu (\nabla \mathbf{u}, \nabla \mathbf{v}) + b^*(\mathbf{u}, \mathbf{u}, \mathbf{v}) - (p, \nabla \cdot \mathbf{v}) = (\mathbf{f}, \mathbf{v}), & \forall \mathbf{v} \in \mathbf{X}, \\ (\nabla \cdot \mathbf{u}, q) = 0, & \forall q \in Q. \end{cases} \quad (2.3)$$

82 To ensure the uniqueness of the solution to (2.3), we make the following regularity assumptions
 83 (see Definition 29 and Remark 10 in [24]):

84 **Assumption 2.1** In (2.1), assume that $\mathbf{f} \in L^2(0, T; \mathbf{L}^2(\Omega))$, $\mathbf{u}^0 \in \mathbf{V}$, $\mathbf{u} \in L^2(0, T; \mathbf{X}) \cap L^\infty(0, T; \mathbf{L}^2(\Omega))$,

85 $\nabla \mathbf{u} \in (L^4(0, T; L^2(\Omega)))^{n \times n}$, $\mathbf{u}_t \in L^2(0, T; \mathbf{X}^*)$, and $p \in L^2(0, T; Q)$.

86 The FE approximation of (2.3) can be written as follows: Find $\mathbf{u}_h \in \mathbf{V}^h$ such that

$$(\mathbf{u}_{h,t}, \mathbf{v}_h) + \nu (\nabla \mathbf{u}_h, \nabla \mathbf{v}_h) + b^*(\mathbf{u}_h, \mathbf{u}_h, \mathbf{v}_h) = (\mathbf{f}, \mathbf{v}_h), \quad \forall \mathbf{v}_h \in \mathbf{V}^h \quad (2.4)$$

87 and $\mathbf{u}_h(\cdot, 0) = \mathbf{u}_h^0 \in \mathbf{V}^h$.

88 2.1 Proper Orthogonal Decomposition

89 We briefly describe the POD method, following [21]. For a detailed presentation, the reader is
90 referred to [6, 13, 29, 30, 35].

91 Consider an ensemble of snapshots $\mathcal{R} := \text{span}\{\mathbf{u}(\cdot, t_0), \dots, \mathbf{u}(\cdot, t_M)\}$, which is a collection of
92 velocity data from either numerical simulation results or experimental observations at time $t_i = i\Delta t$,
93 $i = 0, \dots, M$ and let $\Delta t = \frac{T}{M}$. The POD method seeks a low-dimensional basis $\{\varphi_1, \dots, \varphi_r\}$ in \mathcal{H}
94 that optimally approximates the snapshots in the following sense:

$$\min \frac{1}{M+1} \sum_{\ell=0}^M \left\| \mathbf{u}(\cdot, t_\ell) - \sum_{j=1}^r (\mathbf{u}(\cdot, t_\ell), \varphi_j(\cdot))_{\mathcal{H}} \varphi_j(\cdot) \right\|_{\mathcal{H}}^2 \quad (2.5)$$

95 subject to the conditions that $(\varphi_j, \varphi_i)_{\mathcal{H}} = \delta_{ij}$, $1 \leq i, j \leq r$, where δ_{ij} is the Kronecker delta. To
96 solve (2.5), one can consider the eigenvalue problem

$$K \mathbf{z}_j = \lambda_j \mathbf{z}_j, \quad \text{for } j = 1, \dots, r, \quad (2.6)$$

97 where $K \in \mathbb{R}^{(M+1) \times (M+1)}$ is the snapshot correlation matrix with entries $K_{k\ell} = \frac{1}{M+1} (\mathbf{u}(\cdot, t_\ell), \mathbf{u}(\cdot, t_k))_{\mathcal{H}}$
98 for $\ell, k = 0, \dots, M$, \mathbf{z}_j is the j -th eigenvector, and λ_j is the associated eigenvalue. The eigenvalues
99 are positive and sorted in descending order $\lambda_1 \geq \dots \geq \lambda_r \geq 0$. It can then be shown that the
100 solution of (2.5), the POD basis function, is given by

$$\varphi_j(\cdot) = \frac{1}{\sqrt{\lambda_j}} \sum_{\ell=0}^M (\mathbf{z}_j)_\ell \mathbf{u}(\cdot, t_\ell), \quad 1 \leq j \leq r, \quad (2.7)$$

101 where $(\mathbf{z}_j)_\ell$ is the ℓ -th component of the eigenvector \mathbf{z}_j . It can also be shown that the following

102 error formula holds [13, 21]:

$$\frac{1}{M+1} \sum_{\ell=0}^M \left\| \mathbf{u}(\cdot, t_\ell) - \sum_{j=1}^r (\mathbf{u}(\cdot, t_\ell), \varphi_j(\cdot))_{\mathcal{H}} \varphi_j(\cdot) \right\|_{\mathcal{H}}^2 = \sum_{j=r+1}^d \lambda_j, \quad (2.8)$$

103 where d is the rank of \mathcal{R} .

104 **Remark 2.1** *Since, as shown in (2.7), the POD basis functions are linear combinations of the*
 105 *snapshots, the POD basis functions satisfy the boundary conditions in (2.1) and are solenoidal. If*
 106 *the FE approximations are used as snapshots, the POD basis functions belong to \mathbf{V}^h , which yields*
 107 $\mathbf{X}^r \subset \mathbf{V}^h$.

108 The Galerkin projection-based POD-ROM employs both Galerkin truncation and Galerkin
 109 projection. The former yields an approximation of the velocity field by a linear combination of the
 110 truncated POD basis:

$$\mathbf{u}(\mathbf{x}, t) \approx \mathbf{u}_r(\mathbf{x}, t) \equiv \sum_{j=1}^r a_j(t) \varphi_j(\mathbf{x}), \quad (2.9)$$

111 where $\{a_j(t)\}_{j=1}^r$ are the sought time-varying coefficients representing the POD-Galerkin trajec-
 112 tories. Note that $r \ll N$, where N denotes the number of degrees of freedom in a DNS. Replacing
 113 the velocity \mathbf{u} with \mathbf{u}_r in the NSE (2.1), using the Galerkin method, and projecting the resulted
 114 equations onto the space \mathbf{X}^r , one obtains the *POD-G-ROM* for the NSE: Find $\mathbf{u}_r \in \mathbf{X}^r$ such that

$$\left(\frac{\partial \mathbf{u}_r}{\partial t}, \varphi \right) + \nu (\nabla \mathbf{u}_r, \nabla \varphi) + b^*(\mathbf{u}_r, \mathbf{u}_r, \varphi) = (\mathbf{f}, \varphi), \quad \forall \varphi \in \mathbf{X}^r \quad (2.10)$$

115 and $\mathbf{u}_r(\cdot, 0) = \mathbf{u}_r^0 \in \mathbf{X}^r$. In (2.10), the pressure term vanishes due to the fact that all POD
 116 modes are solenoidal and satisfy the appropriate boundary conditions. The spatial and temporal
 117 discretizations of (2.10) were considered in [22, 26]. Despite its appealing computational efficiency,
 118 the POD-G-ROM (2.10) has generally been limited to laminar flows. To overcome this restriction,
 119 we develop a closure method for the POD-ROM, which stems from the variational multiscale ideas.

120 2.2 Variational Multiscale Method

121 Based on the concept of energy cascade and locality of energy transfer, the VMS method models
 122 the effect of unresolved scales by introducing extra eddy viscosities *to and only to* the resolved small

123 scales [14, 15]. For a standard FE discretization, the separation of scales is generally challenging.
 124 Indeed, unless special care is taken (e.g., mesh adaptivity is used), the FE basis does not include
 125 any a priori information regarding the scales displayed by the underlying problem. Since the POD
 126 basis functions are already listed in descending order of their kinetic energy content, the POD
 127 represents an ideal setting for the VMS methodology. Naturally, we regard the discarded POD
 128 basis functions as unresolved scales, $\{\varphi_1, \dots, \varphi_R\}$ as resolved large scales, and $\{\varphi_{R+1}, \dots, \varphi_r\}$ as
 129 resolved small scales, where $R < r$.

130 We consider the orthogonal projection of \mathbf{L}^2 on \mathbf{L}^R , $P_R : \mathbf{L}^2 \rightarrow \mathbf{L}^R$, defined by

$$(\mathbf{u} - P_R \mathbf{u}, \mathbf{v}_R) = 0, \quad \forall \mathbf{v}_R \in \mathbf{L}^R. \quad (2.11)$$

131 Let $P'_R := \mathbb{I} - P_R$, where \mathbb{I} is the identity operator. We propose the *variational multiscale proper*
 132 *orthogonal decomposition reduced-order model* (P_R -VMS-POD-ROM) for the NSE: Find $\mathbf{u}_r \in \mathbf{X}^r$
 133 such that

$$\left(\frac{\partial \mathbf{u}_r}{\partial t}, \varphi \right) + \nu (\nabla \mathbf{u}_r, \nabla \varphi) + b^*(\mathbf{u}_r, \mathbf{u}_r, \varphi) + \alpha \left(P'_R \nabla \mathbf{u}_r, P'_R \nabla \varphi \right) = (\mathbf{f}, \varphi), \quad \forall \varphi \in \mathbf{X}^r, \quad (2.12)$$

134 where $\alpha > 0$ is a constant EV coefficient and the initial condition is given by the L^2 projection of
 135 \mathbf{u}^0 on \mathbf{X}^r :

$$\mathbf{u}_r(\cdot, 0) = \mathbf{u}_r^0 := \sum_{j=1}^r (\mathbf{u}^0, \varphi_j) \varphi_j. \quad (2.13)$$

136 **Remark 2.2** When $R = r$ or $\alpha = 0$, the P_R -VMS-POD-ROM (2.12) coincides with the standard
 137 POD-G-ROM, since no EV is introduced. When $R = 0$, since EV is added to all modes in the
 138 POD-ROM, the P_R -VMS-POD-ROM (2.12) becomes the mixing-length POD-ROM (ML-POD-
 139 ROM) [3, 37]:

$$\left(\frac{\partial \mathbf{u}_r}{\partial t}, \varphi \right) + \nu (\nabla \mathbf{u}_r, \nabla \varphi) + b^*(\mathbf{u}_r, \mathbf{u}_r, \varphi) + \alpha (\nabla \mathbf{u}_r, \nabla \varphi) = (\mathbf{f}, \varphi), \quad \forall \varphi \in \mathbf{X}^r. \quad (2.14)$$

140 **Remark 2.3** We note that the P_R -VMS-POD-ROM (2.12) is different from the VMS-POD-ROM
 141 introduced in [37]. Indeed, the former uses the operator P'_R and a constant EV coefficient, whereas
 142 the later does not use the operator P'_R and uses a variable EV coefficient.

143 We consider the full discretization of (2.12): We use the backward Euler method with a time
144 step Δt for the time integration and the FE space \mathbb{P}^m with $m \geq 2$ and a mesh size h for the spatial
145 discretization. For $k = 0, \dots, M$, denote the approximation solution of (2.12) at $t_k = k\Delta t$ to be
146 $\mathbf{u}_r^k = \mathbf{u}_{h,r}(t_k)$ and the force at t_k to be $\mathbf{f}^k = \mathbf{f}(t_k)$, respectively. Note that we have dropped the
147 subscript “ h ” in \mathbf{u}_r^k for clarity of notation. The discretized P_R -VMS-POD-ROM then reads: Find
148 $\mathbf{u}_r^k \in \mathbf{X}^r$ such that

$$\left(\frac{\mathbf{u}_r^{k+1} - \mathbf{u}_r^k}{\Delta t}, \boldsymbol{\varphi} \right) + \nu \left(\nabla \mathbf{u}_r^{k+1}, \nabla \boldsymbol{\varphi} \right) + b^* \left(\mathbf{u}_r^{k+1}, \mathbf{u}_r^{k+1}, \boldsymbol{\varphi} \right) + \alpha \left(P'_R \nabla \mathbf{u}_r^{k+1}, P'_R \nabla \boldsymbol{\varphi} \right) = \left(\mathbf{f}^{k+1}, \boldsymbol{\varphi} \right),$$

$$\forall \boldsymbol{\varphi} \in \mathbf{X}^r, k = 0, \dots, M - 1 \quad (2.15)$$

149 and the initial condition given in (2.13): $\mathbf{u}_r^0 = \sum_{j=1}^r (\mathbf{u}^0, \boldsymbol{\varphi}_j) \boldsymbol{\varphi}_j$.

150 In the sequel, we denote by \mathbf{u}^k and \mathbf{u}_h^k the velocity solution of (2.3) and the FE velocity
151 approximation of (2.4) at $t = t_k$, respectively.

152 3 Error Estimates

153 In this section, we present the error analysis for the P_R -VMS-POD-ROM discretization (2.15).
154 We take the FE solutions $\mathbf{u}_h(\cdot, t_i)$, $i = 1, \dots, M$ as snapshots and choose $\mathcal{H} = L^2$ in the POD
155 generation. The error source includes three main components: the spatial FE discretization error,
156 the temporal discretization error, and the POD truncation error. We derive the error estimate
157 in two steps: First, we gather some necessary assumptions and preliminary results in Section 3.1.
158 Then, we present the main result in Section 3.2.

159 In the sequel, we assume C to be a generic constant, which varies in different places, but is
160 always independent of the finite element mesh size h , the finite element order m , the eigenvalues
161 λ_j and the time step size Δt .

162 3.1 Preliminaries

163 We will need the following results for developing a rigorous error estimate:

164 **Assumption 3.1 (finite element error)** *We assume that the FE approximation \mathbf{u}_h of (2.4)*

165 satisfies the following error estimate:

$$\|\mathbf{u} - \mathbf{u}_h\| + h\|\nabla(\mathbf{u} - \mathbf{u}_h)\| \leq C(h^{m+1} + \Delta t). \quad (3.16)$$

166 We also assume the following standard approximation property (see, e.g., page 166 in [24]):

$$\|p - q_h\| \leq Ch^m. \quad (3.17)$$

167 **Remark 3.1** In chapter V of [8], a linearized version of the implicit (backward) Euler scheme
 168 of the NSE (2.1) was considered (see equation (2.2)). Theorem 2.2 in the same chapter proves
 169 (optimal) first order error estimates with respect to the time variable in the L^2 norm. On page 170
 170 it is mentioned that the discretization with respect to the space variable is not considered, since it
 171 has already been thoroughly studied in chapter IV.

172 In [7], the same linearized version of the implicit (backward) Euler scheme as that in equation
 173 (2.2) in chapter V of [8] is considered. The theorem on page 44 in [7] proves (optimal) first order
 174 error estimates with respect to the time variable in the H^1 norm. As in [8], the discretization with
 175 respect to the space variable was not considered.

176 We also note that the implicit (backward) Euler scheme was also considered in [11]. Section
 177 “Time discretization” on page 765 in [11] outlines the derivation of an optimal error estimate with
 178 respect to both space and time. For the explicit (forward) Euler scheme, an (optimal) first order
 179 error estimate with respect to the time variable was proven in [27]. Higher order schemes for the
 180 time discretization of the NSE were analyzed in [4, 5, 8, 12].

181 Thus, although, we are not aware of any reference where estimates (3.16)–(3.17) are actually
 182 proven, the discussion above already shows that this is possible by assembling the results in [7, 8, 11].
 183 Of course, estimates (3.16)–(3.17) have been confirmed by numerous simulations over the years.

184 For the POD approximation, the following POD inverse estimate was proven in Lemma 2 in [21]:

185 **Lemma 3.1** Let φ_i , $i = 1, \dots, r$, be POD basis functions, M_r be the POD mass matrix with entries
 186 $[M_r]_{jk} = (\varphi_k, \varphi_j)$, and S_r be the POD stiffness matrix with entries $[S_r]_{jk} = [M_r]_{jk} + (\nabla\varphi_k, \nabla\varphi_j)$,
 187 where $j, k = 1, \dots, r$. Let $\|\cdot\|_2$ denote the matrix 2-norm. Then, for all $\mathbf{v} \in \mathbf{X}^r$, the following

188 *estimates hold:*

$$\|\mathbf{v}\|_{L^2} \leq \sqrt{\|M_r\|_2 \|S_r^{-1}\|_2} \|\mathbf{v}\|_{H^1}, \quad (3.18)$$

$$\|\mathbf{v}\|_{H^1} \leq \sqrt{\|S_r\|_2 \|M_r^{-1}\|_2} \|\mathbf{v}\|_{L^2}. \quad (3.19)$$

189

190 Note that, since we chose $\mathcal{H} = L^2$ in the POD method, $\|M_r\|_2 = \|M_r^{-1}\|_2 = 1$ in inequalities
191 (3.18)–(3.19).

192 The L^2 norm of the POD projection error is given by (2.8) with $\mathcal{H} = L^2$. The H^1 norm of the
193 POD projection error is given in the following lemma:

194 **Lemma 3.2** *The POD projection error in the H^1 norm satisfies*

$$\frac{1}{M+1} \sum_{\ell=0}^M \left\| \mathbf{u}_h(\cdot, t_\ell) - \sum_{j=1}^r (\mathbf{u}_h(\cdot, t_\ell), \varphi_j(\cdot)) \varphi_j(\cdot) \right\|_1^2 = \sum_{j=r+1}^d \|\varphi_j\|_1^2 \lambda_j. \quad (3.20)$$

195

196 Note that the POD projection error for continuous functions, i.e., the error in the $L^2(0, T; H^1(\Omega))$
197 norm, has been proven in [29] (Theorem 2, page 17). We consider the POD of a discrete function
198 and derive the time averaged POD projection error in the H^1 norm as follows:

199 **Proof** Let $Y = [\mathbf{u}_h(\cdot, t_0), \mathbf{u}_h(\cdot, t_1), \dots, \mathbf{u}_h(\cdot, t_M)]$ be the snapshot matrix. A necessary optimality
200 condition of the POD basis is given by the following eigenvalue problem (see, e.g., [34]):

$$\frac{1}{M+1} Y Y^\top \varphi_j = \lambda_j \varphi_j. \quad (3.21)$$

201 The POD projection error in the H^1 norm satisfies

$$\begin{aligned} & \frac{1}{M+1} \sum_{\ell=0}^M \left\| \mathbf{u}_h(\cdot, t_\ell) - \sum_{j=1}^r (\mathbf{u}_h(\cdot, t_\ell), \varphi_j(\cdot)) \varphi_j(\cdot) \right\|_1^2 \\ &= \frac{1}{M+1} \sum_{\ell=0}^M \left\| \sum_{j=r+1}^d (\mathbf{u}_h(\cdot, t_\ell), \varphi_j) \varphi_j \right\|_1^2 \end{aligned}$$

$$\begin{aligned}
&= \frac{1}{M+1} \sum_{\ell=0}^M \left(\sum_{j=r+1}^d (\mathbf{u}_h(\cdot, t_\ell), \boldsymbol{\varphi}_j) \boldsymbol{\varphi}_j, \sum_{k=r+1}^d (\mathbf{u}_h(\cdot, t_\ell), \boldsymbol{\varphi}_k) \boldsymbol{\varphi}_k \right)_1 \\
&= \frac{1}{M+1} \sum_{\ell=0}^M \sum_{j=r+1}^d \sum_{k=r+1}^d (\mathbf{u}_h(\cdot, t_\ell), \boldsymbol{\varphi}_j) (\mathbf{u}_h(\cdot, t_\ell), \boldsymbol{\varphi}_k) (\boldsymbol{\varphi}_j, \boldsymbol{\varphi}_k)_1 \\
&= \sum_{j=r+1}^d \sum_{k=r+1}^d \left(\frac{1}{M+1} \sum_{\ell=0}^M (\mathbf{u}_h(\cdot, t_\ell), \boldsymbol{\varphi}_j) \mathbf{u}_h(\cdot, t_\ell), \boldsymbol{\varphi}_k \right) (\boldsymbol{\varphi}_j, \boldsymbol{\varphi}_k)_1 \\
&= \sum_{j=r+1}^d \sum_{k=r+1}^d \left(\frac{1}{M+1} Y Y^\top \boldsymbol{\varphi}_j, \boldsymbol{\varphi}_k \right) (\boldsymbol{\varphi}_j, \boldsymbol{\varphi}_k)_1 \\
&\stackrel{(3.21)}{=} \sum_{j=r+1}^d \sum_{k=r+1}^d (\lambda_j \boldsymbol{\varphi}_j, \boldsymbol{\varphi}_k) (\boldsymbol{\varphi}_j, \boldsymbol{\varphi}_k)_1 \\
&= \sum_{j=r+1}^d \sum_{k=r+1}^d \lambda_j \delta_{jk} (\boldsymbol{\varphi}_j, \boldsymbol{\varphi}_k)_1 = \sum_{j=r+1}^d \lambda_j \|\boldsymbol{\varphi}_j\|_1^2, \tag{3.22}
\end{aligned}$$

202 which proves (3.20). □

203 We define the L^2 projection of \mathbf{u} , $P_r \mathbf{u}$, from \mathbf{L}^2 to \mathbf{X}^r as follows:

$$(\mathbf{u} - P_r \mathbf{u}, \boldsymbol{\varphi}_r) = 0, \quad \forall \boldsymbol{\varphi}_r \in \mathbf{X}^r. \tag{3.23}$$

204 We have the following error estimate of the L^2 projection:

205 **Lemma 3.3** *For any $\mathbf{u}^k \in \mathbf{X}$, its L^2 projection, $\mathbf{w}_r^k = P_r \mathbf{u}^k$, satisfies the following error estimates:*

$$\frac{1}{M+1} \sum_{k=0}^M \|\mathbf{u}^k - \mathbf{w}_r^k\|^2 \leq C \left(h^{2m+2} + \Delta t^2 + \sum_{j=r+1}^d \lambda_j \right), \tag{3.24}$$

$$\frac{1}{M+1} \sum_{k=0}^M \|\nabla (\mathbf{u}^k - \mathbf{w}_r^k)\|^2 \leq C \left(h^{2m} + \|S_r\|_2 h^{2m+2} + (1 + \|S_r\|_2) \Delta t^2 + \sum_{j=r+1}^d \|\boldsymbol{\varphi}_j\|_1^2 \lambda_j \right). \tag{3.25}$$

207

208 **Proof** By the definition of the L^2 projection (3.23), we have

$$\|\mathbf{u}^k - \mathbf{w}_r^k\|^2 = (\mathbf{u}^k - \mathbf{w}_r^k, \mathbf{u}^k - \mathbf{w}_r^k) \stackrel{(3.23)}{=} (\mathbf{u}^k - \mathbf{w}_r^k, \mathbf{u} - \mathbf{v}_r^k), \quad \forall \mathbf{v}_r^k \in \mathbf{X}^r. \tag{3.26}$$

209 Using the Cauchy-Schwarz inequality in (3.26), we get

$$\left\| \mathbf{u}^k - \mathbf{w}_r^k \right\| \leq \left\| \mathbf{u}^k - \mathbf{v}_r^k \right\|, \quad \forall \mathbf{v}_r^k \in \mathbf{X}^r. \quad (3.27)$$

210 Decompose $\mathbf{u}^k - \mathbf{v}_r^k = (\mathbf{u}^k - \mathbf{u}_h^k) + (\mathbf{u}_h^k - \mathbf{v}_r^k)$, where \mathbf{u}_h^k is the corresponding FE approximation.

211 Choosing $\mathbf{v}_r^k = P_r \mathbf{u}_h^k := \sum_{j=1}^r (\mathbf{u}_h^k, \boldsymbol{\varphi}_j) \boldsymbol{\varphi}_j$ in (3.27), by the triangle inequality, Assumption 3.1, and

212 the POD projection error estimate (2.8), we have

$$\begin{aligned} \frac{1}{M+1} \sum_{k=0}^M \left\| \mathbf{u}^k - \mathbf{w}_r^k \right\|^2 &\leq \frac{1}{M+1} \sum_{k=0}^M \left(\left\| \mathbf{u}^k - \mathbf{u}_h^k \right\| + \left\| \mathbf{u}_h^k - P_r \mathbf{u}_h^k \right\| \right)^2 \\ &\leq C \left(h^{2m+2} + \Delta t^2 + \sum_{j=r+1}^d \lambda_j \right), \end{aligned} \quad (3.28)$$

213 which proves error estimate (3.24).

214 Using the triangle inequality, Assumption 3.1, the POD inverse estimate (3.19) and Lemma

215 3.2, we obtain

$$\begin{aligned} &\frac{1}{M+1} \sum_{k=0}^M \left\| \nabla (\mathbf{u}^k - \mathbf{w}_r^k) \right\|^2 \\ &\leq \frac{1}{M+1} \sum_{k=0}^M \left(\left\| \nabla (\mathbf{u}^k - \mathbf{u}_h^k) \right\| + \left\| \nabla (\mathbf{u}_h^k - P_r \mathbf{u}_h^k) \right\| + \left\| \nabla (P_r \mathbf{u}_h^k - \mathbf{w}_r^k) \right\| \right)^2 \\ &\leq C \left(h^{2m} + \Delta t^2 + \sum_{j=r+1}^d \|\boldsymbol{\varphi}_j\|_1^2 \lambda_j + \|S_r\|_2 \frac{1}{M+1} \sum_{k=0}^M \left\| P_r \mathbf{u}_h^k - \mathbf{w}_r^k \right\|^2 \right) \\ &\leq C \left(h^{2m} + \Delta t^2 + \sum_{j=r+1}^d \|\boldsymbol{\varphi}_j\|_1^2 \lambda_j + \|S_r\|_2 \frac{1}{M+1} \sum_{k=0}^M \left\| \mathbf{u}_h^k - \mathbf{u}^k \right\|^2 \right) \quad (\mathbf{w}_r^k = P_r \mathbf{u}^k) \\ &\leq C \left(h^{2m} + \|S_r\|_2 h^{2m+2} + (1 + \|S_r\|_2) \Delta t^2 + \sum_{j=r+1}^d \|\boldsymbol{\varphi}_j\|_1^2 \lambda_j \right), \end{aligned} \quad (3.29)$$

216 which proves error estimate (3.25). □

217 We assume that the following estimates, which are similar to (3.24) and (3.25), are also valid:

218 **Assumption 3.2** For any $\mathbf{u}^k \in \mathbf{X}$, its L^2 projection, $\mathbf{w}_r^k = P_r \mathbf{u}^k$, satisfies the following error

219 *estimates:*

$$\left\| \mathbf{u}^k - \mathbf{w}_r^k \right\| \leq C \left(h^{m+1} + \Delta t + \sqrt{\sum_{j=r+1}^d \lambda_j} \right), \quad (3.30)$$

$$\left\| \nabla \left(\mathbf{u}^k - \mathbf{w}_r^k \right) \right\| \leq C \left(h^m + \sqrt{\|S_r\|_2} h^{m+1} + \sqrt{1 + \|S_r\|_2} \Delta t + \sqrt{\sum_{j=r+1}^d \|\varphi_j\|_1^2 \lambda_j} \right) \quad (3.31)$$

220

221 **Remark 3.2** *The assumption that (3.30) and (3.31) hold is quite natural. It simply says that, in*
 222 *the POD truncation error (2.8) and (3.20), no individual term is much larger than the other terms*
 223 *in the sums.*

224 *We also mention that estimates (3.30) and (3.31) would follow directly from the POD truncation*
 225 *error estimates (2.8) and (3.20) if we discarded the $\frac{1}{M+1}$ factor in those estimates. This could be*
 226 *accomplished simply by dropping the $\frac{1}{M+1}$ factor from the snapshot correlation matrix K . In fact,*
 227 *this approach is used in, e.g., [22, 35]. We note, however, that by dropping the $\frac{1}{M+1}$ from the*
 228 *correlation matrix K would most likely increase the magnitudes of the eigenvalues on the RHS of*
 229 *the POD truncation error estimates (2.8) and (3.20).*

230 **Lemma 3.4** (see Lemma 13 and Lemma 14 in [24]) *For any functions $\mathbf{u}, \mathbf{v}, \mathbf{w} \in \mathbf{X}$, the skew-*
 231 *symmetric trilinear form $b^*(\cdot, \cdot, \cdot)$ satisfies*

$$b^*(\mathbf{u}, \mathbf{v}, \mathbf{v}) = 0, \quad (3.32)$$

232

$$b^*(\mathbf{u}, \mathbf{v}, \mathbf{w}) \leq C \|\nabla \mathbf{u}\| \|\nabla \mathbf{v}\| \|\nabla \mathbf{w}\|, \quad (3.33)$$

233 *and a sharper bound*

$$b^*(\mathbf{u}, \mathbf{v}, \mathbf{w}) \leq C \sqrt{\|\mathbf{u}\| \|\nabla \mathbf{u}\|} \|\nabla \mathbf{v}\| \|\nabla \mathbf{w}\|. \quad (3.34)$$

234 We have the following stability result for the P_R -VMS-POD-ROM (2.15):

235 **Lemma 3.5** *The solution of (2.15) satisfies the following bound:*

$$\|\mathbf{u}_r^M\|^2 + \nu \Delta t \sum_{k=0}^{M-1} \|\nabla \mathbf{u}_r^{k+1}\|^2 \leq \|\mathbf{u}_r^0\|^2 + \frac{\Delta t}{\nu} \sum_{k=0}^{M-1} \|\mathbf{f}^{k+1}\|_{-1}^2. \quad (3.35)$$

236

237 **Proof** Choosing $\varphi := \mathbf{u}_r^{k+1}$ in (2.15) and noting that $b^*(\mathbf{u}_r^{k+1}, \mathbf{u}_r^{k+1}, \mathbf{u}_r^{k+1}) = 0$ by (3.32), we obtain

$$\left(\mathbf{u}_r^{k+1} - \mathbf{u}_r^k, \mathbf{u}_r^{k+1} \right) + \nu \Delta t \left(\nabla \mathbf{u}_r^{k+1}, \nabla \mathbf{u}_r^{k+1} \right) + \alpha \Delta t \left(P'_R \nabla \mathbf{u}_r^{k+1}, P'_R \nabla \mathbf{u}_r^{k+1} \right) = \Delta t \left(\mathbf{f}^{k+1}, \mathbf{u}_r^{k+1} \right). \quad (3.36)$$

238 Using the Cauchy-Schwarz inequality, Young's inequality and the fact that the last term on the

239 LHS of (3.36) is positive yields

$$\frac{1}{2} \|\mathbf{u}_r^{k+1}\|^2 - \frac{1}{2} \|\mathbf{u}_r^k\|^2 + \nu \Delta t \|\nabla \mathbf{u}_r^{k+1}\|^2 \leq \Delta t \left(\mathbf{f}^{k+1}, \mathbf{u}_r^{k+1} \right). \quad (3.37)$$

240 Applying the Cauchy-Schwarz inequality and Young's inequality on the RHS of (3.37), we get

$$\frac{1}{2} \|\mathbf{u}_r^{k+1}\|^2 - \frac{1}{2} \|\mathbf{u}_r^k\|^2 + \nu \Delta t \|\nabla \mathbf{u}_r^{k+1}\|^2 \leq \frac{\Delta t}{2\nu} \|\mathbf{f}^{k+1}\|_{-1}^2 + \frac{\nu \Delta t}{2} \|\nabla \mathbf{u}_r^{k+1}\|^2. \quad (3.38)$$

241 Then, the stability estimate (3.35) follows by summing (3.38) from 0 to $M - 1$. \square

242 **Lemma 3.6** *The a priori stability estimate in Lemma 3.5 yields the following bounds:*

$$\|\mathbf{u}_r^{k+1}\|^2 \leq \nu^{-1} \|\mathbf{f}\|_{2,-1}^2 + \|\mathbf{u}_r^0\|^2, \quad \forall k = 0, \dots, M - 1. \quad (3.39)$$

243 3.2 Main Results

244 We are ready to derive the main result of this section, which provides the error estimates for the

245 P_R -VMS-POD-ROM (2.15).

246 **Theorem 3.1** *Under the regularity assumption of the exact solution (Assumption 2.1), the as-*

247 *sumption on the FE approximation (Assumption 3.1) and the assumption on the POD projection*

248 *error (Assumption 3.2), the solution of the P_R -VMS-POD-ROM (2.15) satisfies the following error*

249 *estimate: There exists $\Delta t^* > 0$ such that the inequality*

$$\begin{aligned}
& \left\| \mathbf{u}^M - \mathbf{u}_r^M \right\|^2 + \nu \Delta t \sum_{k=0}^{M-1} \left\| \nabla \left(\mathbf{u}^{k+1} - \mathbf{u}_r^{k+1} \right) \right\|^2 \\
& \leq C \left((1 + \|S_r\|_2 + \|S_R\|_2) \Delta t^2 + h^{2m} + (1 + \|S_r\|_2 + \|S_R\|_2) h^{2m+2} \right. \\
& \quad \left. + \sum_{j=r+1}^d (1 + \|\varphi_j\|_1^2) \lambda_j + \sum_{j=R+1}^d \|\varphi_j\|_1^2 \lambda_j \right)
\end{aligned} \tag{3.40}$$

250 *holds for all $\Delta t < \Delta t^*$.*

251 **Proof** We start deriving the error bound by splitting the error into two terms:

$$\mathbf{u}^{k+1} - \mathbf{u}_r^{k+1} = \left(\mathbf{u}^{k+1} - \mathbf{w}_r^{k+1} \right) - \left(\mathbf{u}_r^{k+1} - \mathbf{w}_r^{k+1} \right) = \boldsymbol{\eta}^{k+1} - \boldsymbol{\phi}_r^{k+1}. \tag{3.41}$$

252 The first term, $\boldsymbol{\eta}^{k+1} = \mathbf{u}^{k+1} - \mathbf{w}_r^{k+1}$, represents the difference between \mathbf{u}^{k+1} and its L^2 projection
253 on \mathbf{X}^r , which has been bounded in Lemma 3.3. The second term, $\boldsymbol{\phi}_r^{k+1}$, is the remainder.

254 Next, we construct the error equation. We first evaluate the weak formulation of the NSE (2.3)
255 at $t = t^{k+1}$ and let $\mathbf{v} = \boldsymbol{\varphi}_r$, then subtract the P_R -VMS-POD-ROM (2.15) from it. We obtain

$$\begin{aligned}
& \left(\mathbf{u}_t^{k+1}, \boldsymbol{\varphi}_r \right) - \left(\frac{\mathbf{u}_r^{k+1} - \mathbf{u}_r^k}{\Delta t}, \boldsymbol{\varphi}_r \right) + \nu \left(\nabla \mathbf{u}^{k+1} - \nabla \mathbf{u}_r^{k+1}, \nabla \boldsymbol{\varphi}_r \right) + b^* \left(\mathbf{u}^{k+1}, \mathbf{u}^{k+1}, \boldsymbol{\varphi}_r \right) \\
& - b^* \left(\mathbf{u}_r^{k+1}, \mathbf{u}_r^{k+1}, \boldsymbol{\varphi}_r \right) - (p, \nabla \cdot \boldsymbol{\varphi}_r) - \alpha \left(P'_R \nabla \mathbf{u}_r^{k+1}, P'_R \nabla \boldsymbol{\varphi}_r \right) = 0, \quad \forall \boldsymbol{\varphi}_r \in \mathbf{X}^r.
\end{aligned} \tag{3.42}$$

256 By subtracting and adding the difference quotient term, $\left(\frac{\mathbf{u}^{k+1} - \mathbf{u}^k}{\Delta t}, \boldsymbol{\varphi}_r \right)$, in (3.42), and applying
257 the decomposition (3.41), we have, for any $\boldsymbol{\varphi}_r \in \mathbf{X}^r$,

$$\begin{aligned}
& \left(\mathbf{u}_t^{k+1} - \frac{\mathbf{u}^{k+1} - \mathbf{u}^k}{\Delta t}, \boldsymbol{\varphi}_r \right) + \frac{1}{\Delta t} \left(\boldsymbol{\eta}^{k+1} - \boldsymbol{\phi}_r^{k+1}, \boldsymbol{\varphi}_r \right) - \frac{1}{\Delta t} \left(\boldsymbol{\eta}^k - \boldsymbol{\phi}_r^k, \boldsymbol{\varphi}_r \right) + \nu \left(\nabla \left(\boldsymbol{\eta}^{k+1} - \boldsymbol{\phi}_r^{k+1} \right), \nabla \boldsymbol{\varphi}_r \right) \\
& + b^* \left(\mathbf{u}^{k+1}, \mathbf{u}^{k+1}, \boldsymbol{\varphi}_r \right) - b^* \left(\mathbf{u}_r^{k+1}, \mathbf{u}_r^{k+1}, \boldsymbol{\varphi}_r \right) - (p, \nabla \cdot \boldsymbol{\varphi}_r) - \alpha \left(P'_R \nabla \mathbf{u}_r^{k+1}, P'_R \nabla \boldsymbol{\varphi}_r \right) = 0.
\end{aligned} \tag{3.43}$$

258 Note that (3.23) implies that $(\boldsymbol{\eta}^k, \boldsymbol{\varphi}_r) = 0$ and $(\boldsymbol{\eta}^{k+1}, \boldsymbol{\varphi}_r) = 0$. Choosing $\boldsymbol{\varphi}_r = \boldsymbol{\phi}_r^{k+1}$ in (3.43) and

259 letting $\mathbf{r}^k = \mathbf{u}_t^{k+1} - \frac{\mathbf{u}^{k+1} - \mathbf{u}^k}{\Delta t}$, we obtain

$$\begin{aligned}
& \frac{1}{\Delta t} (\phi_r^{k+1}, \phi_r^{k+1}) - \frac{1}{\Delta t} (\phi_r^k, \phi_r^{k+1}) + \nu (\nabla \phi_r^{k+1}, \nabla \phi_r^{k+1}) \\
&= (\mathbf{r}^k, \phi_r^{k+1}) + \nu (\nabla \boldsymbol{\eta}^{k+1}, \nabla \phi_r^{k+1}) + b^* (\mathbf{u}^{k+1}, \mathbf{u}^{k+1}, \phi_r^{k+1}) \\
&\quad - b^* (\mathbf{u}_r^{k+1}, \mathbf{u}_r^{k+1}, \phi_r^{k+1}) - (p, \nabla \cdot \phi_r^{k+1}) - \alpha (P'_R \nabla \mathbf{u}_r^{k+1}, P'_R \nabla \phi_r^{k+1}). \tag{3.44}
\end{aligned}$$

260 First, we estimate the LHS of (3.44) by applying the Cauchy-Schwarz inequality and Young's
261 inequality:

$$\begin{aligned}
\text{LHS} &= \frac{1}{\Delta t} \|\phi_r^{k+1}\|^2 - \frac{1}{\Delta t} (\phi_r^k, \phi_r^{k+1}) + \nu \|\nabla \phi_r^{k+1}\|^2 \\
&\geq \frac{1}{2\Delta t} \left(\|\phi_r^{k+1}\|^2 - \|\phi_r^k\|^2 \right) + \nu \|\nabla \phi_r^{k+1}\|^2. \tag{3.45}
\end{aligned}$$

262 Multiplying by $2\Delta t$ both sides of inequality (3.45) and using the result in (3.44), we obtain

$$\begin{aligned}
& \|\phi_r^{k+1}\|^2 - \|\phi_r^k\|^2 + 2\nu\Delta t \|\nabla \phi_r^{k+1}\|^2 \\
&\leq 2\Delta t (\mathbf{r}^k, \phi_r^{k+1}) + 2\nu\Delta t (\nabla \boldsymbol{\eta}^{k+1}, \nabla \phi_r^{k+1}) + 2\Delta t b^* (\mathbf{u}^{k+1}, \mathbf{u}^{k+1}, \phi_r^{k+1}) \\
&\quad - 2\Delta t b^* (\mathbf{u}_r^{k+1}, \mathbf{u}_r^{k+1}, \phi_r^{k+1}) - 2\Delta t (p, \nabla \cdot \phi_r^{k+1}) - 2\alpha\Delta t (P'_R \nabla \mathbf{u}_r^{k+1}, P'_R \nabla \phi_r^{k+1}) \tag{3.46}
\end{aligned}$$

263 Next, we estimate the terms on the RHS of (3.46) one by one. Using the Cauchy-Schwarz inequality
264 and Young's inequality, we get

$$(\mathbf{r}^k, \phi_r^{k+1}) \leq \|\mathbf{r}^k\|_{-1} \|\nabla \phi_r^{k+1}\| \leq \frac{c_1^{-1}}{4} \|\mathbf{r}^k\|_{-1}^2 + c_1 \|\nabla \phi_r^{k+1}\|^2, \tag{3.47}$$

265

$$\nu (\nabla \boldsymbol{\eta}^{k+1}, \nabla \phi_r^{k+1}) \leq \nu \|\nabla \boldsymbol{\eta}^{k+1}\| \|\nabla \phi_r^{k+1}\| \leq \frac{c_2^{-1}\nu}{4} \|\nabla \boldsymbol{\eta}^{k+1}\|^2 + c_2\nu \|\nabla \phi_r^{k+1}\|^2. \tag{3.48}$$

266 The nonlinear terms in (3.46) can be written as follows:

$$\begin{aligned}
& b^* \left(\mathbf{u}^{k+1}, \mathbf{u}^{k+1}, \phi_r^{k+1} \right) - b^* \left(\mathbf{u}_r^{k+1}, \mathbf{u}_r^{k+1}, \phi_r^{k+1} \right) \\
&= b^* \left(\mathbf{u}_r^{k+1}, \boldsymbol{\eta}^{k+1} - \phi_r^{k+1}, \phi_r^{k+1} \right) + b^* \left(\boldsymbol{\eta}^{k+1} - \phi_r^{k+1}, \mathbf{u}^{k+1}, \phi_r^{k+1} \right) \\
&= b^* \left(\mathbf{u}_r^{k+1}, \boldsymbol{\eta}^{k+1}, \phi_r^{k+1} \right) + b^* \left(\boldsymbol{\eta}^{k+1}, \mathbf{u}^{k+1}, \phi_r^{k+1} \right) - b^* \left(\phi_r^{k+1}, \mathbf{u}^{k+1}, \phi_r^{k+1} \right), \quad (3.49)
\end{aligned}$$

267 where we have used $b^* \left(\mathbf{u}^{k+1}, \phi_r^{k+1}, \phi_r^{k+1} \right) = 0$, which follows from (3.32). Next, we estimate each
268 term on the RHS of (3.49). Since $\mathbf{u}_r^{k+1}, \boldsymbol{\eta}^{k+1}, \phi_r^{k+1} \in \mathbf{X}$, we can apply the standard bounds for the
269 trilinear form $b^* (\cdot, \cdot, \cdot)$ and use Young's inequality:

$$\begin{aligned}
b^* \left(\mathbf{u}_r^{k+1}, \boldsymbol{\eta}^{k+1}, \phi_r^{k+1} \right) &\stackrel{(3.34)}{\leq} C \left\| \mathbf{u}_r^{k+1} \right\|^{1/2} \left\| \nabla \mathbf{u}_r^{k+1} \right\|^{1/2} \left\| \nabla \boldsymbol{\eta}^{k+1} \right\| \left\| \nabla \phi_r^{k+1} \right\| \\
&\leq \frac{1}{4c_3} C^2 \left\| \mathbf{u}_r^{k+1} \right\| \left\| \nabla \mathbf{u}_r^{k+1} \right\| \left\| \nabla \boldsymbol{\eta}^{k+1} \right\|^2 + c_3 \left\| \nabla \phi_r^{k+1} \right\|^2; \quad (3.50)
\end{aligned}$$

270

$$\begin{aligned}
b^* \left(\boldsymbol{\eta}^{k+1}, \mathbf{u}^{k+1}, \phi_r^{k+1} \right) &\stackrel{(3.33)}{\leq} C \left\| \nabla \boldsymbol{\eta}^{k+1} \right\| \left\| \nabla \mathbf{u}^{k+1} \right\| \left\| \nabla \phi_r^{k+1} \right\| \\
&\leq \frac{1}{4c_4} C^2 \left\| \nabla \mathbf{u}^{k+1} \right\|^2 \left\| \nabla \boldsymbol{\eta}^{k+1} \right\|^2 + c_4 \left\| \nabla \phi_r^{k+1} \right\|^2; \quad (3.51)
\end{aligned}$$

271

$$\begin{aligned}
b^* \left(\phi_r^{k+1}, \mathbf{u}^{k+1}, \phi_r^{k+1} \right) &\stackrel{(3.34)}{\leq} C \left\| \phi_r^{k+1} \right\|^{\frac{1}{2}} \left\| \nabla \phi_r^{k+1} \right\|^{\frac{1}{2}} \left\| \nabla \mathbf{u}^{k+1} \right\| \left\| \nabla \phi_r^{k+1} \right\| \\
&= C \left\| \phi_r^{k+1} \right\|^{\frac{1}{2}} \left\| \nabla \mathbf{u}^{k+1} \right\| \left\| \nabla \phi_r^{k+1} \right\|^{\frac{3}{2}} \\
&\leq C \frac{c_5^{-3}}{4} \left\| \nabla \mathbf{u}^{k+1} \right\|^4 \left\| \phi_r^{k+1} \right\|^2 + C \frac{3c_5}{4} \left\| \nabla \phi_r^{k+1} \right\|^2. \quad (3.52)
\end{aligned}$$

272 Since $\phi_r^{k+1} \in \mathbf{X}^r \subset \mathbf{V}^h$, the pressure term on the RHS of (3.46) can be written as

$$-\left(p, \nabla \cdot \phi_r^{k+1} \right) = -\left(p - q_h, \nabla \cdot \phi_r^{k+1} \right), \quad (3.53)$$

273 where q_h is any function in Q^h . Thus, the pressure term can be estimated as follows by the
274 Cauchy-Schwarz inequality and Young's inequality:

$$-\left(p, \nabla \cdot \phi_r^{k+1} \right) \leq \frac{1}{4c_6} \|p - q_h\|^2 + c_6 \left\| \nabla \phi_r^{k+1} \right\|^2. \quad (3.54)$$

275 The last term on the RHS of (3.46) can be estimated as follows:

$$\begin{aligned}
& -\alpha \left(P'_R \nabla \mathbf{u}_r^{k+1}, P'_R \nabla \phi_r^{k+1} \right) \\
&= \alpha \left(P'_R \nabla \mathbf{u}^{k+1} - P'_R \nabla \mathbf{u}_r^{k+1}, P'_R \nabla \phi_r^{k+1} \right) - \alpha \left(P'_R \nabla \mathbf{u}^{k+1}, P'_R \nabla \phi_r^{k+1} \right) \\
&= \alpha \left(P'_R \nabla \boldsymbol{\eta}^{k+1}, P'_R \nabla \phi_r^{k+1} \right) - \alpha \left(P'_R \nabla \phi_r^{k+1}, P'_R \nabla \phi_r^{k+1} \right) - \alpha \left(P'_R \nabla \mathbf{u}^{k+1}, P'_R \nabla \phi_r^{k+1} \right) \\
&\leq \alpha \left\| P'_R \nabla \boldsymbol{\eta}^{k+1} \right\| \cdot \left\| P'_R \nabla \phi_r^{k+1} \right\| - \alpha \left\| P'_R \nabla \phi_r^{k+1} \right\|^2 - \alpha \left(P'_R \nabla \mathbf{u}^{k+1}, P'_R \nabla \phi_r^{k+1} \right) \\
&\leq \alpha \left(\left\| P'_R \nabla \boldsymbol{\eta}^{k+1} \right\|^2 + \frac{1}{4} \left\| P'_R \nabla \phi_r^{k+1} \right\|^2 \right) - \alpha \left\| P'_R \nabla \phi_r^{k+1} \right\|^2 + \alpha \left(\left\| P'_R \nabla \mathbf{u}^{k+1} \right\|^2 + \frac{1}{4} \left\| P'_R \nabla \phi_r^{k+1} \right\|^2 \right) \\
&\leq \alpha \left\| P'_R \nabla \boldsymbol{\eta}^{k+1} \right\|^2 - \frac{\alpha}{2} \left\| P'_R \nabla \phi_r^{k+1} \right\|^2 + \alpha \left\| P'_R \nabla \mathbf{u}^{k+1} \right\|^2. \tag{3.55}
\end{aligned}$$

276 Note that, since P_R is the L^2 projection of \mathbf{L}^2 on \mathbf{L}^R , we get

$$\left\| P'_R \nabla \boldsymbol{\eta}^{k+1} \right\| \leq \left\| \nabla \boldsymbol{\eta}^{k+1} \right\|.$$

277 Choosing $c_1 = c_3 = c_4 = c_6 = \frac{\nu}{12}$, $c_2 = \frac{1}{12}$ and $c_5 = \frac{\nu}{9C}$, then substituting the above inequalities in

278 (3.46), we obtain

$$\begin{aligned}
& \left\| \phi_r^{k+1} \right\|^2 - \left\| \phi_r^k \right\|^2 + \nu \Delta t \left\| \nabla \phi_r^{k+1} \right\|^2 + \alpha \Delta t \left\| P'_R \nabla \phi_r^{k+1} \right\|^2 \\
&\leq \frac{6\Delta t}{\nu} \left\| \mathbf{r}^k \right\|_{-1}^2 + 6\nu \Delta t \left\| \nabla \boldsymbol{\eta}^{k+1} \right\|^2 + \frac{6\Delta t}{\nu} C^2 \left\| \mathbf{u}_r^{k+1} \right\| \left\| \nabla \mathbf{u}_r^{k+1} \right\| \left\| \nabla \boldsymbol{\eta}^{k+1} \right\|^2 + \frac{6\Delta t}{\nu} C^2 \left\| \nabla \mathbf{u}^{k+1} \right\|^2 \left\| \nabla \boldsymbol{\eta}^{k+1} \right\|^2 \\
&+ \frac{C^4 9^3 \nu^{-3} \Delta t}{2} \left\| \nabla \mathbf{u}^{k+1} \right\|^4 \left\| \phi_r^{k+1} \right\|^2 + \frac{6\Delta t}{\nu} \left\| p - q_h \right\|^2 + 2\alpha \Delta t \left\| \nabla \boldsymbol{\eta}^{k+1} \right\|^2 + 2\alpha \Delta t \left\| P'_R \nabla \mathbf{u}^{k+1} \right\|^2. \tag{3.56}
\end{aligned}$$

279 Summing (3.56) from $k = 0$ to $k = M - 1$, we have

$$\begin{aligned}
& \left\| \phi_r^M \right\|^2 + \nu \Delta t \sum_{k=0}^{M-1} \left\| \nabla \phi_r^{k+1} \right\|^2 + \alpha \Delta t \sum_{k=0}^{M-1} \left\| P'_R \nabla \phi_r^{k+1} \right\|^2 \\
&\leq \left\| \phi_r^0 \right\|^2 + \frac{6\Delta t}{\nu} \sum_{k=0}^{M-1} \left\| \mathbf{r}^k \right\|_{-1}^2 + 6\nu \Delta t \sum_{k=0}^{M-1} \left\| \nabla \boldsymbol{\eta}^{k+1} \right\|^2 + \frac{6\Delta t}{\nu} C^2 \sum_{k=0}^{M-1} \left\| \mathbf{u}_r^{k+1} \right\| \left\| \nabla \mathbf{u}_r^{k+1} \right\| \left\| \nabla \boldsymbol{\eta}^{k+1} \right\|^2 \\
&+ \frac{6\Delta t}{\nu} C^2 \sum_{k=0}^{M-1} \left\| \nabla \mathbf{u}^{k+1} \right\|^2 \left\| \nabla \boldsymbol{\eta}^{k+1} \right\|^2 + \frac{C^4 9^3 \nu^{-3} \Delta t}{2} \sum_{k=0}^{M-1} \left\| \nabla \mathbf{u}^{k+1} \right\|^4 \left\| \phi_r^{k+1} \right\|^2 \\
&+ \frac{6\Delta t}{\nu} \sum_{k=0}^{M-1} \left\| p - q_h \right\|^2 + 2\alpha \Delta t \sum_{k=0}^{M-1} \left\| \nabla \boldsymbol{\eta}^{k+1} \right\|^2 + 2\alpha \Delta t \sum_{k=0}^{M-1} \left\| P'_R \nabla \mathbf{u}^{k+1} \right\|^2. \tag{3.57}
\end{aligned}$$

280 Next, we estimate each term on the RHS of (3.57).

281 The first term vanishes since $\mathbf{u}_r^0 = \mathbf{w}_r^0$ (see (2.13)).

282 By using the Poincaré-Friedrichs' inequality, the second term on the RHS of (3.57) can be
 283 estimated as follows (see, e.g., [16]):

$$\Delta t \sum_{k=0}^{M-1} \|\mathbf{r}^k\|_{-1}^2 \leq C \Delta t \sum_{k=0}^{M-1} \|\mathbf{r}^k\|^2 \leq C \Delta t^2 \|\mathbf{u}_{tt}\|_{2,2}^2. \quad (3.58)$$

284 Using (3.25), the third and eighth terms on the RHS of (3.57) can be estimated as follows:

$$\Delta t \sum_{k=0}^{M-1} \|\nabla \eta^{k+1}\|^2 \leq C \left(h^{2m} + \|S_r\|_2 h^{2m+2} + (1 + \|S_r\|_2) \Delta t^2 + \sum_{j=r+1}^d \|\varphi_j\|_1^2 \lambda_j \right). \quad (3.59)$$

285 To estimate the fourth term on the RHS of (3.57), we use Lemma 3.6

$$\begin{aligned} & \Delta t \sum_{k=0}^{M-1} \|\mathbf{u}_r^{k+1}\| \|\nabla \mathbf{u}_r^{k+1}\| \|\nabla \eta^{k+1}\|^2 \\ (3.39) \quad & \leq \left(\nu^{-1/2} \|\mathbf{f}\|_{2,-1} + \|\mathbf{u}_r^0\| \right) \Delta t \sum_{k=0}^{M-1} \|\nabla \mathbf{u}_r^{k+1}\| \|\nabla \eta^{k+1}\|^2 \\ (3.31) \quad & \leq C \left(\nu^{-1/2} \|\mathbf{f}\|_{2,-1} + \|\mathbf{u}_r^0\| \right) \Delta t \sum_{k=0}^{M-1} \|\nabla \mathbf{u}_r^{k+1}\| \left(h^{2m} + \|S_r\|_2 h^{2m+2} + (1 + \|S_r\|_2) \Delta t^2 \right. \\ & \quad \left. + \sum_{j=r+1}^d \|\varphi_j\|_1^2 \lambda_j \right). \end{aligned} \quad (3.60)$$

286 We note that we used estimate (3.31) in the derivation of (3.60); using (3.25) would not have been
 287 enough for the asymptotic convergence of (3.60).

288 The fifth term on the RHS of (3.57) can be bounded as follows:

$$\begin{aligned} & \Delta t \sum_{k=0}^{M-1} \|\nabla \mathbf{u}^{k+1}\|^2 \|\nabla \eta^{k+1}\|^2 \\ (3.31) \quad & \leq C \Delta t \sum_{k=0}^{M-1} \|\nabla \mathbf{u}^{k+1}\|^2 \left(h^{2m} + \|S_r\|_2 h^{2m+2} + (1 + \|S_r\|_2) \Delta t^2 + \sum_{j=r+1}^d \|\varphi_j\|_1^2 \lambda_j \right) \end{aligned} \quad (3.61)$$

289 The seventh term on the RHS of (3.57) has been bounded by the approximation property (3.17)
 290 in Assumption 3.1.

291

Using (2.2c), we have the following error bound of the last term on the RHS of (3.57):

$$\begin{aligned}
& \Delta t \sum_{k=0}^{M-1} \left\| P'_R \nabla \mathbf{u}^{k+1} \right\|^2 = \Delta t \sum_{k=0}^{M-1} \left\| \nabla \mathbf{u}^{k+1} - P_R \nabla \mathbf{u}^{k+1} \right\|^2 \\
& \leq C \frac{1}{M} \sum_{k=0}^{M-1} \inf_{\mathbf{v}_R \in \mathbf{X}_R} \left\| \nabla \mathbf{u}^{k+1} - \nabla \mathbf{v}_R \right\|^2 \leq C \frac{1}{M} \sum_{k=0}^{M-1} \left\| \nabla \mathbf{u}^{k+1} - \nabla \mathbf{w}_R^{k+1} \right\|^2 \\
& \stackrel{(3.25)}{\leq} C \left(h^{2m} + \|S_R\|_2 h^{2m+2} + (1 + \|S_R\|_2) \Delta t^2 + \sum_{j=R+1}^d \|\varphi_j\|_1^2 \lambda_j \right). \tag{3.62}
\end{aligned}$$

292

Collecting (3.58)-(3.62) and letting $d = C(6\nu + 2\alpha) + 6C^3\nu^{-1}(\nu^{-\frac{1}{2}}\|f\|_{2,-1} + \|\mathbf{u}_r^0\|)\|\nabla \mathbf{u}_r\|_{1,0} +$

293

$6C^3\nu^{-1}\|\nabla \mathbf{u}_r\|_{2,0}^2$, $d_1 = \frac{C^4 g^3 \nu^{-3}}{2}$, $d_2 = 6C\nu^{-1}(\|\mathbf{u}_{tt}\|_{2,2}^2 + 1) + 2C\alpha + d$, $d_3 = 6C\nu^{-1} + 2C\alpha + d$, and

294

$d_4 = 2\alpha C$, equation (3.57) becomes

$$\begin{aligned}
& \|\phi_r^M\|^2 + \nu \Delta t \sum_{k=0}^{M-1} \left\| \nabla \phi_r^{k+1} \right\|^2 + \alpha \Delta t \sum_{k=0}^{M-1} \left\| P'_R \nabla \phi_r^{k+1} \right\|^2 \\
& \leq d_1 \Delta t \sum_{k=0}^{M-1} \left\| \nabla \mathbf{u}^{k+1} \right\|^4 \left\| \phi_r^{k+1} \right\|^2 + d_2 \Delta t^2 + d \|S_r\|_2 \Delta t^2 + d_3 h^{2m} + d \|S_r\|_2 h^{2m+2} \\
& + d \sum_{j=r+1}^d \|\varphi_j\|_1^2 \lambda_j + d_4 \left(\|S_R\|_2 \Delta t^2 + \|S_R\|_2 h^{2m+2} + \sum_{j=R+1}^d \|\varphi_j\|_1^2 \lambda_j \right). \tag{3.63}
\end{aligned}$$

295

If $\Delta t < \Delta t^* := d_1 \|\nabla \mathbf{u}\|_{4,0}^4$, the discrete Gronwall lemma (see Lemma 27 in [24] and also [12])

296

implies the following inequality:

$$\begin{aligned}
& \|\phi_r^M\|^2 + \nu \Delta t \sum_{k=0}^{M-1} \left\| \nabla \phi_r^{k+1} \right\|^2 + \alpha \Delta t \sum_{k=0}^{M-1} \left\| P'_R \nabla \phi_r^{k+1} \right\|^2 \\
& \leq C^* \left(d_2 \Delta t^2 + d \|S_r\|_2 \Delta t^2 + d_3 h^{2m} + d \|S_r\|_2 h^{2m+2} + d \sum_{j=r+1}^d \|\varphi_j\|_1^2 \lambda_j \right. \\
& \left. + d_4 \left(\|S_R\|_2 \Delta t^2 + \|S_R\|_2 h^{2m+2} + \sum_{j=R+1}^d \|\varphi_j\|_1^2 \lambda_j \right) \right), \tag{3.64}
\end{aligned}$$

297

where $C^* = e^{d_1 \Delta t \sum_{k=0}^{M-1} \|\nabla \mathbf{u}^{k+1}\|^4}$.

298

By dropping the third term on the LHS of (3.64) and using (3.30), (3.25), and the triangle

299 inequality, we get

$$\begin{aligned}
& \|\mathbf{u}^M - \mathbf{u}_r^M\|^2 + \nu \Delta t \sum_{k=0}^{M-1} \left\| \nabla \left(\mathbf{u}^{k+1} - \mathbf{u}_r^{k+1} \right) \right\|^2 \\
& \leq C \left((1 + \|S_r\|_2 + \|S_R\|_2) \Delta t^2 + h^{2m} + (1 + \|S_r\|_2 + \|S_R\|_2) h^{2m+2} \right. \\
& \quad \left. + \sum_{j=r+1}^d (1 + \|\varphi_j\|_1^2) \lambda_j + \sum_{j=R+1}^d \|\varphi_j\|_1^2 \lambda_j \right). \tag{3.65}
\end{aligned}$$

300 This completes the proof. □

301 4 Numerical Experiments

302 The goal of this section is twofold. In Section 4.1, we investigate the physical accuracy of the
303 P_R -VMS-POD-ROM. To this end, we test the model in the numerical simulation of a 3D flow past
304 a circular cylinder at $\text{Re} = 1000$. The P_R -VMS-POD-ROM is compared with the POD-G-ROM
305 and the ML-POD-ROM in which a constant EV is employed [3, 37]. All the numerical results are
306 benchmarked against DNS data. A parallel CFD solver is employed to generate the DNS data [1].
307 For details on the numerical discretization, the reader is referred to the appendix in [36]. To assess
308 the physical accuracy of the the POD-ROMs, two criteria are employed: (i) the time evolution
309 of the POD coefficients, which measures the instantaneous behavior of the models; and (ii) the
310 energy spectrum, which measures the average behavior of the models. In Section 4.2, we illustrate
311 numerically the theoretical error estimates in Theorem 3.1. Specifically, we investigate the error's
312 asymptotic behavior with respect to the time step, Δt , and the POD contribution to the error
313 introduced by the EV term, $\sum_{j=R+1}^d \|\varphi_j\|_1^2 \lambda_j$.

314 4.1 Physical Accuracy

315 In this section, we test the P_R -VMS-POD-ROM in the numerical simulation of a 3D flow past a
316 circular cylinder at $\text{Re} = 1000$. By using the method of snapshots [30], we compute the POD basis
317 $\{\varphi_1, \dots, \varphi_d\}$ from 1000 snapshots of the velocity field over 15 shedding cycles, i.e., $t \in [0, 75]$ (see
318 Figure 1). These POD modes are then interpolated onto a structured quadratic FE mesh with
319 nodes coinciding with the nodes used in the original DNS finite volume discretization. Six POD

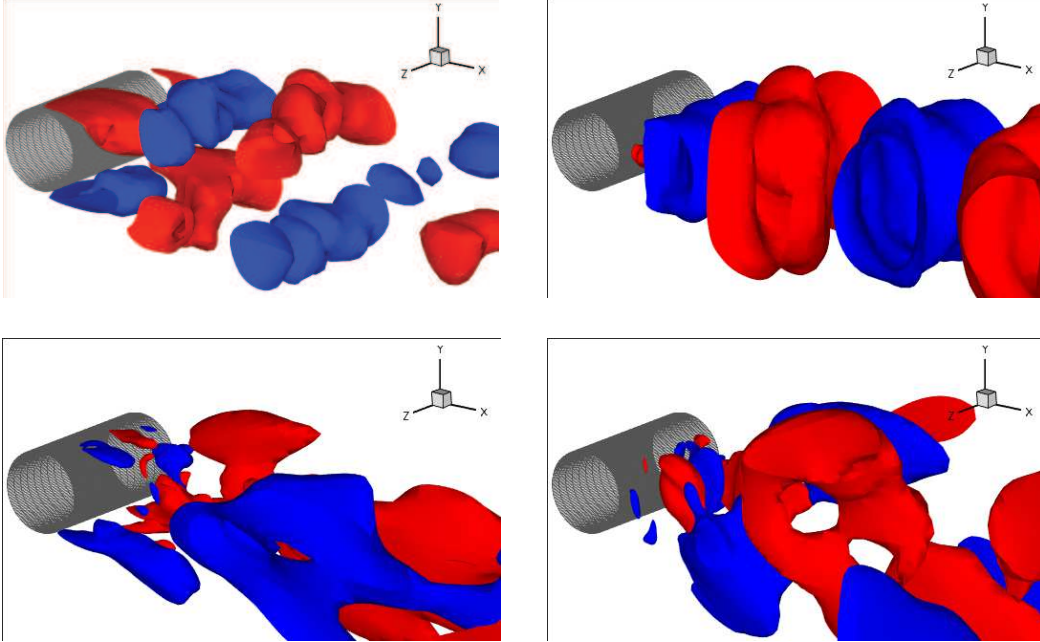


Figure 1: 3D flow past a cylinder at $Re = 1000$. First streamwise POD mode (top left), first normal POD mode (top right), third streamwise POD mode (bottom left), and third normal POD mode (bottom right).

320 basis functions ($r=6$) are then used in all POD-ROMs that we investigate next. These first six
321 POD modes capture 84% of the system's energy. For all these POD-ROMs, the time discretization
322 was effected by using the backward Euler method with $\Delta t = 7.5 \times 10^{-3}$. We emphasize that
323 the time interval used in the simulations of POD-ROMs is *four times larger* than that in which
324 snapshots are generated, i.e., $t \in [0, 300]$. Thus, the *predictive* capabilities of the POD-ROMs are
325 investigated. In Figure 2, the time evolutions of the POD coefficients a_1 and a_4 are plotted. The
326 other POD coefficients have a similar qualitative behavior, so, for clarity, they are not included in
327 our plots. To determine the EV constants in the ML-POD-ROM and the P_R -VMS-POD-ROM, we
328 run the models on the short time interval $[0, 15]$ with several different values for the EV constants
329 and choose the value that yields the results that are closest to the DNS results. This approach
330 yields the following values for the EV constants: $\alpha = 3 \times 10^{-3}$ for the ML-POD-ROM (2.14) and
331 $\alpha = 3.5 \times 10^{-3}$ for the P_R -VMS-POD-ROM (2.12) when $R = 1$. We emphasize that these EV
332 constant values are optimal only on the short time interval tested, and they might actually be
333 nonoptimal on the entire time interval $[0, 300]$ on which the POD-ROMs are tested. Thus, this
334 heuristic procedure ensures some fairness in the numerical comparison of the three POD-ROMs.

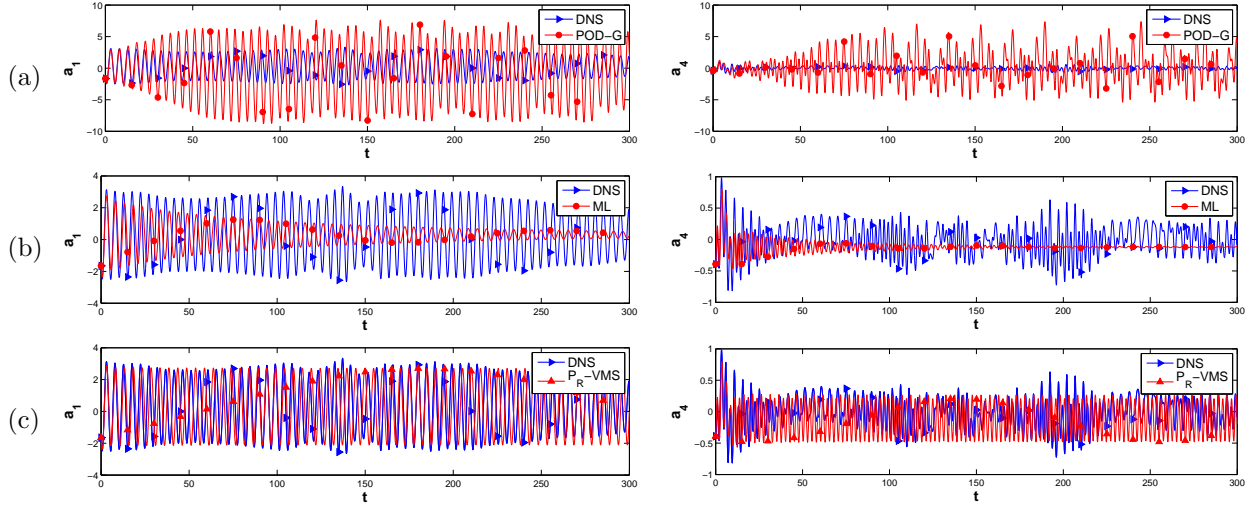


Figure 2: 3D flow past a cylinder at $Re = 1000$. Temporal evolution of POD coefficients $a_1(\cdot)$ and $a_4(\cdot)$ over the time interval $[0, 300]$ for POD-G-ROM (a), ML-POD-ROM (b), and P_R -VMS-POD-ROM (c).

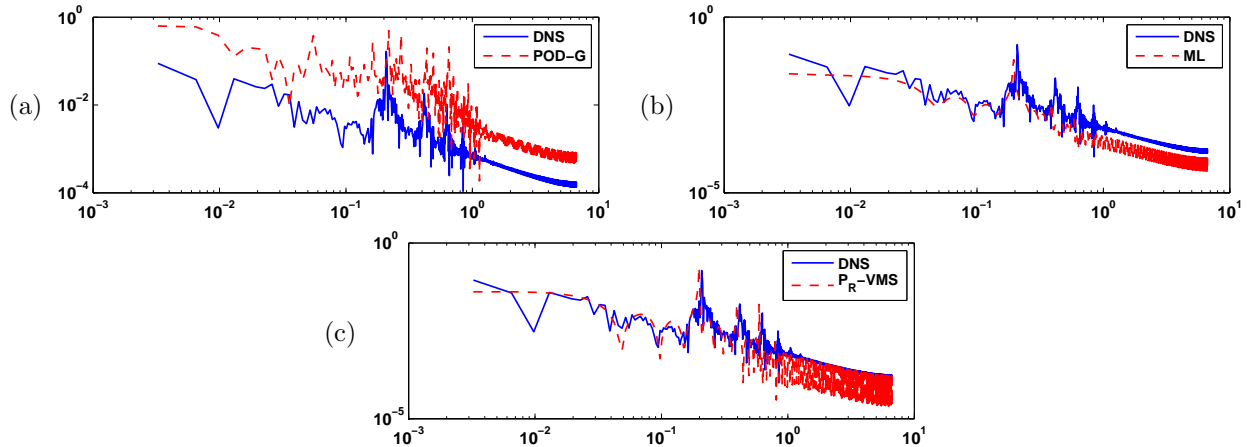


Figure 3: 3D flow past a cylinder at $Re = 1000$. Comparison of energy spectrum of DNS with that of POD-G-ROM (a), ML-POD-ROM (b), and P_R -VMS-POD-ROM (c).

335 The POD-G-ROM (2.10) performs poorly, although it is computationally efficient (its CPU
 336 time is 118 s). Indeed, the amplitude of the temporal evolution of the POD coefficient $a_4(\cdot)$ is
 337 *nine times larger* than that for the DNS projection. The ML-POD-ROM's time evolutions of
 338 the POD coefficients a_1 and a_4 are also inaccurate. Specifically, although the time evolution at
 339 the beginning of the simulation (where the EV constant α was chosen) is relatively accurate,
 340 the accuracy significantly degrades toward the end of the simulation. For example, as shown in
 341 Figure 2(b), the magnitude of a_4 at the end of the simulation is only one eighth of that of the DNS.

342 The P_R -VMS-POD-ROM yields more accurate time evolutions than both the POD-G-ROM and
 343 the ML-POD-ROM for both a_1 and a_4 , as shown in Figure 2(c). The P_R -VMS-POD-ROM is as
 344 efficient as POD-G-ROM, its CPU time being 129 s.

345 Figure 3 presents the energy spectra of the three POD-ROMs. The three energy spectra are
 346 compared with the DNS energy spectrum. For the energy spectra, we use the approach in [37]
 347 and we calculate the average kinetic energy of the nodes in the cube with side 0.1 centered at
 348 the probe (0.9992, 0.3575, 1.0625). The energy spectrum of the POD-G-ROM (2.10) overestimates
 349 the energy spectrum of the DNS. The energy spectrum of the ML-POD-ROM (2.14), on the other
 350 hand, underestimates the the energy spectrum of the DNS, especially at the higher frequencies.
 351 Although it displays high oscillations at the higher frequencies, the P_R -VMS-POD-ROM (2.12) has
 352 a more accurate spectrum than both the POD-G-ROM (2.10) and the ML-POD-ROM (2.14).

353 4.2 Numerical Accuracy

354 In this section, we test the P_R -VMS-POD-ROM in the numerical simulation of the 2D incompress-
 355 ible NSE (2.1). The exact velocity, $\mathbf{u} = (u, v)$, has components $u = \frac{2}{\pi} \arctan(-500(y - t)) \sin(\pi y)$,
 356 $v = \frac{2}{\pi} \arctan(-500(x - t)) \sin(\pi x)$, and the exact pressure is given by $p = 0$. The inverse of the
 357 Reynolds number is $\nu = 10^{-3}$ and the forcing term is chosen to match the exact solution. Taylor-
 358 Hood FEs are used to discretize the spatial domain $[0, 1] \times [0, 1]$. We collect snapshots over the
 359 time interval $[0, 1]$ at every $\Delta T = 10^{-2}$ by recording the exact values of u and v on the FE mesh
 360 with the mesh size $h = 1/64$. After applying the method of snapshots, we obtain a POD basis set
 361 with the dimension of 101.

362 In POD-ROMs, the backward Euler method is employed for time integration over the same time
 363 interval. To verify the numerical error of the P_R -VMS-POD-ROM (2.12) with respect to the time
 364 step, Δt , we choose $h = 1/64$, $r = 99$, $R = 95$ and $\alpha = 10^{-3}$. With this choice, h^{2m} is on the order
 365 of 10^{-8} , and $\sum_{j=r+1}^d \|\varphi_j\|_1^2 \lambda_j$ and $\sum_{j=R+1}^d \|\varphi_j\|_1^2 \lambda_j$ are on the order of 10^{-4} . Thus, asymptotically, the
 366 time discretization error dominates the total error in the theoretical error estimate (3.40). The
 367 total error in the L^2 norm at the final time, $\mathcal{E} = \|\mathbf{u}^M - \mathbf{u}_r^M\|$, is listed in Table 1 for decreasing
 368 values of the time step, Δt . A linear regression between \mathcal{E} and Δt (see Figure 4) shows that the rate
 369 of convergence of the numerical error is nearly linear with respect to the time step, as predicted

370 by the theoretical error estimate (3.40):

$$\mathcal{E} = 2.66(\Delta t)^{0.96}.$$

Table 1: The P_R -VMS-POD-ROM with $h = 1/64$, $r = 99$, $R = 95$, and $\alpha = 10^{-3}$. The total error in the L^2 -norm at the final time, $\|\mathbf{u}^M - \mathbf{u}_r^M\|$, for decreasing values of the time step, Δt .

Δt	$\ \mathbf{u}^M - \mathbf{u}_r^M\ $
5×10^{-3}	2.31×10^{-2}
2.5×10^{-3}	6.30×10^{-3}
1.25×10^{-3}	3.46×10^{-3}
6.25×10^{-4}	2.05×10^{-3}
3.13×10^{-4}	1.45×10^{-3}

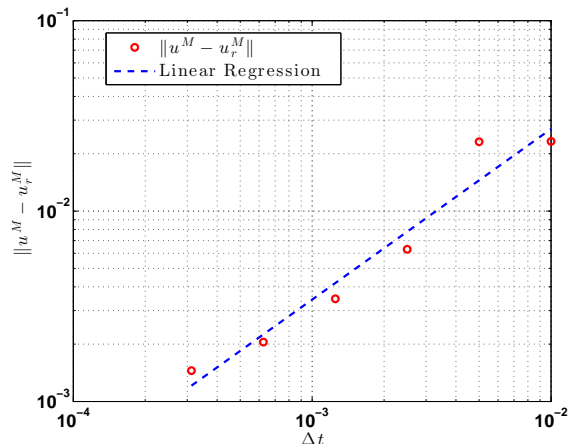


Figure 4: The P_R -VMS-POD-ROM with $h = 1/64$, $r = 99$, $R = 95$ and $\alpha = 10^{-3}$. A linear regression between the total error in the L^2 -norm at the final time, \mathcal{E} , and the time step, Δt , is nearly linear : $\mathcal{E} \sim \mathcal{O}((\Delta t)^{0.96})$.

371 To verify the numerical error of the P_R -VMS-POD-ROM with respect to R , we choose $h = 1/64$,
 372 $\Delta t = 10^{-4}$, and $r = 99$. With this choice, h^{2m} and Δt^2 are on the order of 10^{-8} and $\sum_{j=r+1}^d \|\varphi_j\|_1^2 \lambda_j$
 373 is on the order of 10^{-4} . Thus, asymptotically, the POD contribution to the error introduced by the
 374 EV term, $\sum_{j=R+1}^d \|\varphi_j\|_1^2 \lambda_j$, dominates the total error in the theoretical error estimate (3.40). For
 375 a fixed $\alpha = 10^{-3}$, total error in the L^2 norm at the final time, $\mathcal{E}^2 = \|\mathbf{u}^M - \mathbf{u}_r^M\|^2$, is listed in Table
 376 2 for increasing values of R . A linear regression between \mathcal{E}^2 and $\sum_{j=R+1}^d \|\varphi_j\|_1^2 \lambda_j$ (see Figure 5)
 377 shows an almost quadratic rate of convergence, which is higher than the linear rate of convergence
 378 predicted by the theoretical error estimate (3.40):

$$\mathcal{E}^2 = c \left(\sum_{j=R+1}^d \|\varphi_j\|_1^2 \lambda_j \right)^{1.94},$$

379 where $c = 3.2 \times 10^{-9}$.

Table 2: The P_R -VMS-POD-ROM with $h = 1/64$, $\Delta t = 10^{-4}$, $r = 99$, and $\alpha = 10^{-3}$. The square of the total error in the L^2 -norm at the final time, $\|\mathbf{u}^M - \mathbf{u}_r^M\|^2$, for increasing values of R .

R	$\sum_{j=R+1}^d \ \varphi_j\ _1^2 \lambda_j$	$\ \mathbf{u}^M - \mathbf{u}_r^M\ ^2$
6	2.18×10^2	1.43×10^{-4}
10	1.99×10^2	1.05×10^{-4}
16	1.73×10^2	6.70×10^{-5}
24	1.43×10^2	4.04×10^{-5}
34	1.10×10^2	2.39×10^{-5}
45	7.80×10^1	1.54×10^{-5}
56	5.37×10^1	8.92×10^{-6}

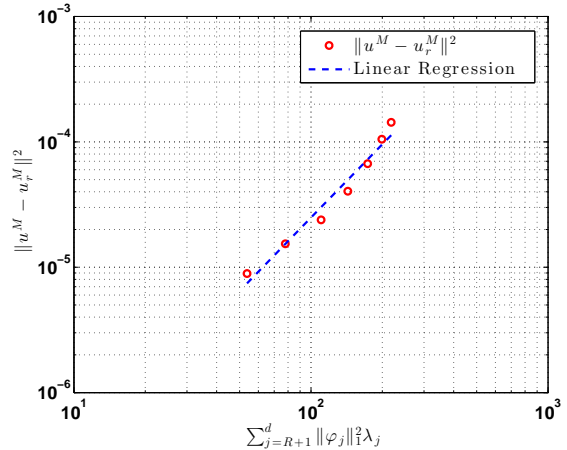


Figure 5: The P_R -VMS-POD-ROM with $h = 1/64$, $\Delta t = 10^{-4}$, $r = 99$, and $\alpha = 10^{-3}$. A linear regression between the square of the total error in the L^2 -norm at the final time, \mathcal{E}^2 , and the the POD contribution to the error introduced by the EV term, $\sum_{j=R+1}^d \|\varphi_j\|_1^2 \lambda_j$: $\mathcal{E}^2 \sim \mathcal{O}\left(\left(\sum_{j=R+1}^d \|\varphi_j\|_1^2 \lambda_j\right)^{1.94}\right)$.

5 Conclusions

In this paper, we proposed a new ROM for the numerical simulation of turbulent incompressible fluid flows. This model, denoted P_R -VMS-POD-ROM, utilizes a VMS method and a projection operator to model the effect of the high index POD modes that are not included in the ROM. A rigorous error estimate was derived for the full discretization of the P_R -VMS-POD-ROM. All the contributions to the total error were considered: the spatial discretization error (due to the FE discretization), the temporal discretization error (due to the backward Euler method), and the POD truncation error. The P_R -VMS-POD-ROM was also tested in the numerical simulation of a 3D flow past a circular cylinder at $Re = 1000$. The numerical tests showed that the P_R -VMS-POD-ROM is both physically accurate and computationally efficient. Furthermore, the numerical results illustrated the theoretical error estimates.

We note that the EV coefficient α in the P_R -VMS-POD-ROM is simply chosen to be a constant. We plan to extend this theoretical and numerical study by considering more accurate choices for the EV coefficients, such as the Smagorinsky model [37, 33]. We also plan to investigate this model in more complex physical settings, such as the Boussinesq equations [28]. Finally, we plan

395 to reduce the computational cost of the P_R -VMS-POD-ROM by a different treatment of the time
396 discretization of the VMS term.

397 Acknowledgement

398 The first author acknowledges the partial support by the National Science Foundation (DMS-
399 0513542 and OCE-0620464). The second author was supported by the Institute for Mathematics
400 and its Applications with funds provided by the National Science Foundation. We thank the
401 anonymous reviewers for their constructive comments, which helped improve the manuscript.

402 References

- 403 [1] I. Akhtar. *Parallel simulations, reduced-order modeling, and feedback control of vortex shedding using*
404 *fluidic actuators*. PhD thesis, Virginia Tech, 2008.
- 405 [2] J. A. Atwell and B. B. King. Reduced order controllers for spatially distributed systems via proper
406 orthogonal decomposition. *SIAM Journal on Scientific Computing*, 26(1):128–151 (electronic), 2004.
- 407 [3] N. Aubry, P. Holmes, J. L. Lumley, and E. Stone. The dynamics of coherent structures in the wall
408 region of a turbulent boundary layer. *Journal of Fluid Mechanics*, 192:115–173, 1988.
- 409 [4] G. A. Baker. Galerkin approximations for the Navier-Stokes equations. Technical report, Harvard
410 University, 1976.
- 411 [5] G. A. Baker, V. Dougalis, and O. Karakashian. On a higher order accurate fully discrete Galerkin
412 approximation to the Navier-Stokes equations. *Mathematics of Computation*, 39(160):339–375, 1982.
- 413 [6] D. Chapelle, A. Gariah, and J. Sainte-Marie. Galerkin approximation with proper orthogonal decompo-
414 sition: new error estimates and illustrative examples. *ESAIM: Mathematical Modelling and Numerical*
415 *Analysis*, 46(04):731–757, 2012.
- 416 [7] T. Geveci. On the convergence of a time discretization scheme for the Navier-Stokes equations. *Math-*
417 *ematics of Computation*, 53(187):43–53, 1989.
- 418 [8] V. Girault and P.-A. Raviart. *Finite element approximation of the Navier-Stokes equations*, volume
419 749 of *Lecture Notes in Mathematics*. Springer-Verlag, Berlin, 1979.
- 420 [9] J.-L. Guermond. Stabilization of Galerkin approximations of transport equations by subgrid modeling.
421 *M2AN. Mathematical Modelling and Numerical Analysis*, 33(6):1293–1316, 1999.

- 422 [10] J.-L. Guermond. Stabilisation par viscosité de sous-maille pour l'approximation de Galerkin des
423 opérateurs linéaires monotones. *Comptes Rendus Mathématique*, 328:617–622, 1999.
- 424 [11] J. G. Heywood and R. Rannacher. Finite element approximation of the nonstationary Navier-Stokes
425 problem, part II: Stability of solutions and error estimates uniform in time. *SIAM Journal on Numerical
426 Analysis*, 23(4):750–777, 1986.
- 427 [12] J. G. Heywood and R. Rannacher. Finite-element approximation of the nonstationary Navier-Stokes
428 problem, part IV: Error analysis for second-order time discretization. *SIAM Journal on Numerical
429 Analysis*, 27(2):353–384, 1990.
- 430 [13] P. Holmes, J. L. Lumley, and G. Berkooz. *Turbulence, Coherent Structures, Dynamical Systems and
431 Symmetry*. Cambridge University Press, Cambridge, UK, 1996.
- 432 [14] T. J. R. Hughes, L. Mazzei, A. Oberai, and A. Wray. The multiscale formulation of large eddy simula-
433 tion: Decay of homogeneous isotropic turbulence. *Physics of Fluids*, 13(2):505–512, 2001.
- 434 [15] T. J. R. Hughes, A. Oberai, and L. Mazzei. Large eddy simulation of turbulent channel flows by the
435 variational multiscale method. *Physics of Fluids*, 13(6):1784–1799, 2001.
- 436 [16] T. Iliescu and Z. Wang. Variational multiscale proper orthogonal decomposition: Convection-dominated
437 convection-diffusion-reaction equations. *Mathematics of Computation*, 82:1357–1378, 2013.
- 438 [17] V. John and S. Kaya. A finite element variational multiscale method for the Navier–Stokes equations.
439 *SIAM Journal on Scientific Computing*, 26:1485–1503, 2005.
- 440 [18] V. John and S. Kaya. Finite element error analysis of a variational multiscale method for the Navier-
441 Stokes equations. *Advances in Computational Mathematics*, 28(1):43–61, 2008.
- 442 [19] V. John, S. Kaya, and A. Kindl. Finite element error analysis for a projection-based variational
443 multiscale method with nonlinear eddy viscosity. *Journal of Mathematical Analysis and Applications*,
444 344(2):627–641, 2008.
- 445 [20] V. John, S. Kaya, and W. Layton. A two-level variational multiscale method for convection-dominated
446 convection-diffusion equations. *Computational Methods in Applied Mechanical Engineering*, 195(33-
447 36):4594–4603, 2006.
- 448 [21] K. Kunisch and S. Volkwein. Galerkin proper orthogonal decomposition methods for parabolic problems.
449 *Numerische Mathematik*, 90(1):117–148, 2001.
- 450 [22] K. Kunisch and S. Volkwein. Galerkin proper orthogonal decomposition methods for a general equation
451 in fluid dynamics. *SIAM Journal on Numerical Analysis*, 40(2):492–515 (electronic), 2002.

- 452 [23] W. J. Layton. A connection between subgrid scale eddy viscosity and mixed methods. *Applied Mathe-*
453 *matics and Computation*, 133:147–157, 2002.
- 454 [24] W. J. Layton. *Introduction to the numerical analysis of incompressible viscous flows*, volume 6. Society
455 for Industrial and Applied Mathematics (SIAM), 2008.
- 456 [25] J. L. Lumley. The structure of inhomogeneous turbulent flows. In A.M. Yaglom, editor, *Atmospheric*
457 *Turbulence and Radio Wave Propagation*, pages 166–178, 1967.
- 458 [26] Z. Luo, J. Chen, I. M. Navon, and X. Yang. Mixed finite element formulation and error estimates based
459 on proper orthogonal decomposition for the nonstationary Navier-Stokes equations. *SIAM Journal on*
460 *Numerical Analysis*, 47(1):1–19, 2008.
- 461 [27] R. Rannacher. *Stable finite element solutions to nonlinear parabolic problems of Navier-Stokes type*,
462 pages 301–309. R. Glowinski and J. L. Lions, eds., North-Holland, Amsterdam, 1982.
- 463 [28] S. S. Ravindran. Error analysis for Galerkin POD approximation of the nonstationary Boussinesq
464 equations. *Numerical Methods for Partial Differential Equations*, 27(6):1639–1665, 2010.
- 465 [29] J. R. Singler. New POD error expressions, error bounds, and asymptotic results for reduced order
466 model of parabolic PDEs. *Preprint*.
- 467 [30] L. Sirovich. Turbulence and the dynamics of coherent structures. I. Coherent structures. *Quarterly of*
468 *Applied Mathematics*, 45(3):561–571, 1987.
- 469 [31] L. Sirovich. Turbulence and the dynamics of coherent structures. II. Symmetries and transformations.
470 *Quarterly of Applied Mathematics*, 45(3):573–582, 1987.
- 471 [32] L. Sirovich. Turbulence and the dynamics of coherent structures. III. Dynamics and scaling. *Quarterly*
472 *of Applied Mathematics*, 45(3):583–590, 1987.
- 473 [33] S. Ullmann and J. Lang. A POD-Galerkin reduced model with updated coefficients for Smagorinsky
474 LES. In J. C. F. Pereira and A. Sequeira, editors, *V European Conference on Computational Fluid*
475 *Dynamics, ECCOMAS CFD 2010*, Lisbon, Portugal, June 2010.
- 476 [34] K. Kunisch; S. Volkwein. Control of the Burgers equation by a reduced-order approach using proper
477 orthogonal decomposition. *Journal of Optimization Theory and Application*, 102(2):345–371, 1999.
- 478 [35] S. Volkwein. Model reduction using proper orthogonal decomposition. [http://www.math.uni-](http://www.math.uni-konstanz.de/numerik/personen/volkwein/teaching/POD-Vorlesung.pdf)
479 [konstanz.de/numerik/personen/volkwein/teaching/POD-Vorlesung.pdf](http://www.math.uni-konstanz.de/numerik/personen/volkwein/teaching/POD-Vorlesung.pdf), 2011.
- 480 [36] Z. Wang, I. Akhtar, J. Borggaard, and T. Iliescu. Two-level discretizations of nonlinear closure models
481 for proper orthogonal decomposition. *Journal of Computational Physics*, 230:126–146, 2011.

482 [37] Z. Wang, I. Akhtar, J. Borggaard, and T. Ilescu. Proper orthogonal decomposition closure models for
483 turbulent flows: A numerical comparison. *Computational Methods in Applied Mechanical Engineering*,
484 237–240:10–26, 2012.